Large-Scale Simulations of Advanced Materials and Nanoscale Devices

J. Bernholc, M. Buongiorno Nardelli, W. Lu, V. Meunier, W.G. Schmidt, S. Wang, and Q. Zhao
Department of Physics, North Carolina State University, Raleigh, NC
Sponsor: Office of Naval Research, Arlington, VA
bernholc@ncsu.edu

Abstract

Recent advances in theoretical methods and parallel supercomputing allow for reliable ab initio simulations of the properties of complex materials. We describe two current applications: pyro- and piezoelectric properties of BN nanotubes and optical signatures of organic molecules on Si(001) surface. BN nanotubes turn out to be excellent piezoelectrics, with response values significantly greater than those of piezoelectric polymers. However, their symmetry leads to exact cancellation of the total spontaneous polarization in ideal, isolated nanotubes. Breaking of this symmetry induces spontaneous polarization comparable to those of wurtzite semiconductors. Turning to organics on Si(100), we calculated the atomic structure and the optical signatures of a cyclopentene overlayer on Si(001). Cyclopentene can be used to attach a variety of organic molecules to Si devices, including DNA, and can therefore form a basis of a sensor structure. The spectra turn out to be highly structure-dependent and can therefore be used to monitor interface formation.

1. Introduction

In this report we describe two applications of our large-scale *ab initio* methodology: a search for robust piezo-and pyroelectric materials and an investigation of the initial stages of the formation of an extensible Si-organic interface.

Piezo- and pyroelectric materials for modern technological applications should display an excellent piezo-electric response, combined with high mechanical stability and low environmental impact. Existing materials, which can be broadly divided into the families of ceramics and polymers, can only partially fulfill the above requirements. Lead zirconate titanate, (PZT) ceramics, for example, are strong piezo- and pyroelectrics[1,2] but, unfortunately, they are also brittle, heavy and toxic. On the other hand, polymers like polyvinylidene fluoride, (PVDF) are lightweight, flexible and virtually inert, but their polar properties are an order of magnitude weaker than those of PZT.[3] Polymeric materials have already found extensive usage in a variety of transducers and sensors, including sonar equipment. However, it would clearly be desirable to find materials with improved electric response and strength, while preserving the desirable properties of, e.g., PVDF. We have thus carried out an in-depth investigation of the spontaneous polarization and piezoelectricity in boron nitride nanotubes, (BNNTs), in order to estimate their potential usefulness in various pyro- and piezoelectric device applications, and to understand the interplay between symmetry and polarization in nanotubular systems.

BNNTs, broadly investigated since their initial prediction[4] and succeeding discovery,[5] are already well known for their excellent mechanical properties.[6] However, unlike carbon nanotubes, most of BN structures are non-centrosymmetric and polar, which might suggest the existence of non-zero spontaneous polarization fields. Recently, these properties have been partially explored by Mele and Král, using a model electronic Hamiltonian.[7] They predicted that BNNTs are piezo- and pyroelectric, with the direction of the spontaneous electric field that changes with the index of the tubes. The *ab initio* calculations presented in this paper provide a much fuller description and show that BNNT systems are indeed excellent lightweight piezoelectrics, with comparable or better piezoelectric response and superior mechanical properties than in piezoelectric polymers. However, contrary to the conclusions of Ref. 7, our combined Berry phase and Wannier function, (WF) analysis demonstrates that electronic polarization in BNNTs does not change its direction but rather grows monotonically with the increasing diameter of the tube. Furthermore, the electronic and ionic spontaneous polarizations in BNNTs cancel exactly and these systems are pyroelectric only if

Proceedings of the 2003 User Group Conference (DoD_UGC'03)
0-7695-1953-9/03 $17.00 © 2003 IEEE

their intrinsic helical symmetry is broken by, *e.g.*, inter-tube interactions or elastic distortions.

The, (001) surface of silicon is the starting point for the fabrication of most microelectronic devices. Therefore, Si surface reactions with metals, hydrogen, oxygen and halogens have been intensively studied in the past.[8] However, in recent years there is an increasing interest in developing methods for coupling microelectronics with organic-based structures for applications such as nonlinear optics, thin-film displays, lithography, and molecular electronics. For this reason, much effort has been devoted to the preparation and characterization of ultra-thin organic layers on Si(001) surfaces.[9–19] Some adsorption geometries have also been probed by cluster [18] and density-functional calculations.[20,21] Organic overlayers may also facilitate the attachment of biomolecules, such as DNA, to the semiconductor surface.[22,23]

Chemisorption of organic molecules on Si(001) is typically accompanied by their fragmentation. Alkenes, however, can bond to the surface by breaking the π bonds of the alkene and of the Si dimers, and forming two new σ bonds. This mechanism has been exploited to prepare ordered organic overlayers of cyclopentene,[9,17] 1,5-cyclooctadiene, [11,17] 1,3,5,7-cyclooctatetraene[12] and 1,3-dienes[13] on the Si substrate. These systems have novel and often extremely interesting properties. The chemisorption of bifunctional compounds such as 1,5-cyclooctadiene, for example, leads to the formation of an ordered array of carbon-carbon double bonds, which can then be utilized for further reactions. [17]

The adsorption of cyclopentene, (C_5H_8) on Si leads to what can be considered a prototypical alkene-Si(001) interface. It is experimentally well characterized by scanning tunneling microscopy, (STM) and by infrared and core-level spectroscopies.[9,11,16,17] From experiment, [9] two possible scenarios have been suggested for the reaction between Si(001) and a cyclopentene molecule: a [2+2] cycloaddition reaction, leaving the Si dimer intact, and an insertion reaction, where the Si dimer is broken, (dimer-cleaved model). The reactions that leave the dimer intact, result in 'dimerized' models and lead to a chemically saturated, but highly strained interface geometry.[24] On the other hand, the dimer cleavage reaction releases the strain, but leaves unpaired electrons in the Si dangling bonds. Below, we present first-principles calculations of the structural and optical properties of the monolayer cyclopentene covered Si(001) surface. In addition to the interface models discussed above, we consider the effects of hydrogenation on interface structure and properties. We find that the addition of hydrogen atoms stabilizes and smooths the interface, which could be beneficial for further reactions. The optical anisotropy of Si(001): C_5H_8 is found to be remarkably sensitive to details of the chemical bonding and can be used to distinguish between alternative chemical and structural models.

2. Methodology

Most of the calculations were performed using our *ab initio* multigrid-based total-energy method, employing a real-space grid as a basis. [28] The exchange-correlation contributions were represented by the Perdew and Zunger parameterization,[26] and the generalized gradient approximation, (GGA) corrections [27] were computed for surfaces. The electron-ion interactions were represented by nonlocal, norm-conserving pseudo potentials. [28]

Computing the polarization in materials requires special attention, because standard periodic boundary conditions calculations cannot deal with surface charges and thus with non-zero polarization fields inside the solid. The appropriate generalization utilizes a Berry-phase formulation,[29,30] which accounts for the adiabatic "current" that flows when a system is transformed from a non-polar to a polar phase. The transformation must leave the system insulating. Using λ, as the transformation parameter, the polarization difference between two states of a system $\Delta\boldsymbol{P} = \boldsymbol{P}^{(\lambda_1)} - \boldsymbol{P}^{(\lambda_0)}$ is computed by splitting $\boldsymbol{P}^{(\lambda)}$ into two parts: $\boldsymbol{P}_{ion}^{(\lambda)}$ and, $\boldsymbol{P}_{el}^{(\lambda)}$ corresponding to the ionic and electronic contributions respectively.

The relevant expressions are:

$$\boldsymbol{P}^{(\lambda)} = \boldsymbol{P}_{ion}^{(\lambda)} + \boldsymbol{P}_{el}^{(\lambda)}$$
$$= \frac{e}{V}\sum_{\tau} Z_{\tau}^{(\lambda)}\boldsymbol{r}_{\tau}^{(\lambda)} - \frac{2ie}{8\pi^3}\sum_{i\,occ}\int_{\mathrm{BZ}} \mathrm{d}\boldsymbol{k}\left(\mathrm{u}_{i\boldsymbol{k}}^{(\lambda)}\middle|\nabla_{i\boldsymbol{k}}\middle|u_{i\boldsymbol{k}}^{(\lambda)}\right), \quad (1)$$

where V is the volume of the unit cell, Z_τ and $\boldsymbol{r}_\tau$ are the charge and position of the π-th atom in the cell, and $u_{i\boldsymbol{k}}$ are the occupied cell-periodic Bloch states of the system. For the electronic part, an electronic phase $\varphi_\alpha^{(\lambda)}$, (Berry phase) defined modulo 2π can be introduced as

$$\varphi_\alpha^{(\lambda)} = V\,\boldsymbol{G}_\alpha \cdot \boldsymbol{P}_{el}^{(\lambda)} / e\,, \quad (2)$$

where $\boldsymbol{G}_\alpha$ is the reciprocal lattice vector in the direction α. Similarly, one can construct an angular variable for the ionic part, called in what follows the "ionic" phase.

Alternatively, the electronic polarization of a system can be expressed in terms of the centers of charge of the Wannier functions of its occupied bands[29,30]:

$$\boldsymbol{P}_{el}^{(\lambda)} = \frac{2e}{V}\sum_i \int \mathbf{r}\left|W_i^{(\lambda)}(\mathbf{r})\right|^2 d\mathbf{r} = -\frac{2e}{V}\sum_i \left(\mathbf{r}_i^{(\lambda)}\right), \quad (3)$$

where the Wannier function, (WF) $W_i^{(\lambda)}$, (**r**) is constructed from the Bloch eigenstates $u_{ik}^{(\lambda)}$ of band *i* using the unitary transformation

$$W_i(\mathbf{r}) = \frac{V}{(2\pi)^3} \int_{BZ} e^{ikr} u_{ik}(\mathbf{r})\, d\mathbf{k}\,, \qquad (4)$$

and $\left(\mathbf{r}_i^{(\lambda)}\right)$ is the center of charge for the WF $W_i^{(\lambda)}$. In both methods presented above, $\boldsymbol{P}_{el}^{(\lambda)}$ can be obtained only modulo $2e\boldsymbol{R}/V$ due to the arbitrariness in the choice of the phases of the Bloch functions. However, the difference in polarization $\Delta\boldsymbol{P}$ is well defined if $|\Delta\boldsymbol{P}_{el}| \ll |2e\boldsymbol{R}/V|$. The same indetermination issues apply to $\boldsymbol{P}_{ion}^{(\lambda)}$.[31]

Turning to calculations of optical properties of surfaces, we calculated the reflection anisotropy spectra in the independent-particle approximation.[32,33] To avoid spurious contributions from the bottom surface of the slab, a linear cutoff function was used.[34] The self-energy effects in the surface optical spectra were approximated by the scissors operator approach. We have described the details of our approach in previous papers, and our computational procedures for calculating optical spectra are by now well established, with many successful applications to complex reconstructions on III-V surfaces and steps on Si surfaces.

3. Results and Discussion

3.1. Polarization and piezoelectricity in BN nanotubes.

We first focus on Berry phase calculations in zigzag BNNTs. The ionic part of the polarization, presented in Figure 1, is large and directly proportional to the nanotube's index. This is in contrast, for instance, to the corresponding wurtzite III-V and II-VI systems,[35,36] where the spontaneous polarization can be viewed as the difference between the polarizations of the wurtzite, (polar) and zincblende, (nonpolar) geometries. Since these configurations become geometrically distinct only in the second shell of neighbors, their ionic phases are very close. The major contribution to the spontaneous polarization in wurtzite materials is then due to the difference between the electronic polarizations, (which are 0.04–0.08 C/m^2), while in BNNTs both the *ionic* and the *electronic* contributions are essential.

The ionic phase differences $\Delta\varphi_{ion}$ between the polar and nonpolar configurations of zigzag nanotubes were evaluated via the virtual crystal approximation. The inset in Figure 1 shows the results obtained by a simple lattice summation over the ionic charges with the phases translated into the $[-\pi, \pi]$ interval. The phases plotted in the main graph were "unfolded" by eliminating all the 2π discontinuities and setting the phase of the nonpolar reference configuration to zero. For the unfolded phases, as the diameter of a nanotube increases, *i.e.*, as another hexagon is added around the circumference of the tube, the ionic phase goes up by $\pi/3$, so that the total ionic phase for a, (*n;* 0) BN nanotube amounts to $n\pi/3$.

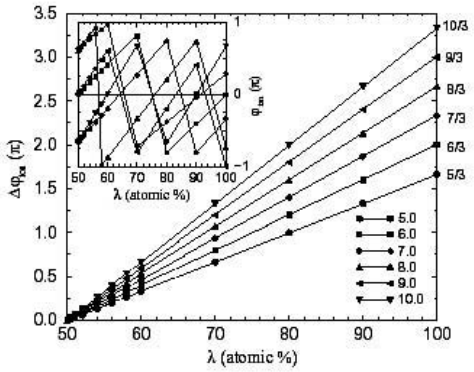

Figure. 1. Ionic-phase difference between the polar and nonpolar configurations for zigzag nanotubes; the ionic phase of the nonpolar configuration is set to zero. Inset: ionic phases wrapped into the [–*π*, *π*] interval. Phases are given in units of *π*.

In Figure 2 we show the electronic-phase differences $\Delta\varphi_{el}$ between the polar and nonpolar configurations for zigzag nanotubes. These data suggest a natural division of the nanotubes into three families with different $\Delta\varphi_{el}$: $\pi/3$ for $n = 3l - 1$, $-\pi/3$ for $n = 3l + 1$, and $-\pi$ for $n = 3l$ where *l* is an integer,[37] which is similar to the result obtained by Mele and Král.[7] However, the existence of such three classes of behavior is surprising, given that the ionic character of the electronic charge density, (associated with the B-N bond) does not change with the nanotube index. Additionally, there is an important difference between our results and those of Ref. 7, where the electronic polarization of heteropolar nanotubes was studied within a simple π-orbital tight-binding, (π-TB) approximation. In Ref. 7, the "$n = 3l$" family has a zero electronic phase instead of $-\pi$.

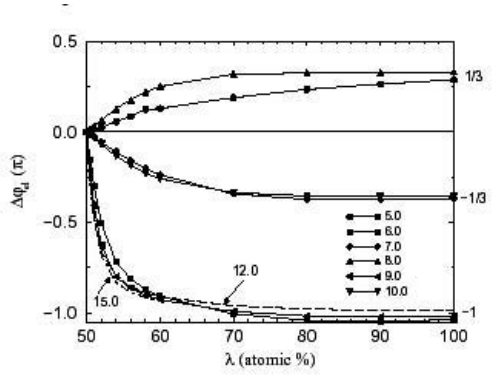

Figure 2. Electronic-phase differences between the polar and nonpolar configurations for zigzag nanotubes.

This discrepancy is due to the ambiguity of the definition of electronic polarization as a multivalued quantity,[31] which can assume a lattice of values corresponding to Berry phases that differ by arbitrary multiples of 2π. Unlike the ionic phase model, where discontinuities in $\varphi_{ion}(\lambda)$ can be easily monitored, Berry phase calculations always produce phases that are smoothly folded into the $[-\pi, \pi]$ interval and cannot be extrapolated. To obtain an unambiguous determination of the spontaneous polarization of BNNTs of arbitrary diameters, one has to compute the polarization in a different way, using the centers of charge of the WFs of the occupied bands, (Eq. 3).

The results of the maximally localized WF calculations for BNNTs are summarized in Figure 3, where examples of the WFs for C and BN zigzag nanotubes of arbitrary diameter are shown, together with a schematic drawing that illustrates the shift of the Wannier centers in the adiabatic transformation from C to BN. Since

$$\boldsymbol{P}_{el}^{(BN)} = \frac{2e}{V}\sum_i \left(\mathbf{r}_i^{(BN)} - \mathbf{r}_i^{(C)}\right) \qquad (5)$$

the magnitude of the shift of the centers is directly proportional to the electronic polarization of the BNNT with respect to the nonpolar CNT.

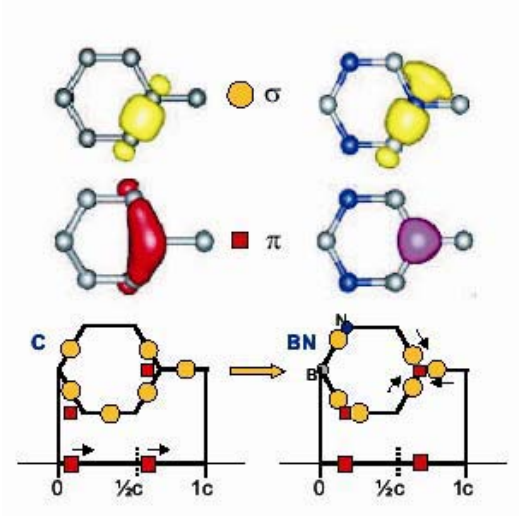

Figure 3. Upper panel: Examples of Wannier functions, (WF) of the *σ* and *π* occupied bands of C, (left panel) and BN, (right panel) nanotubes. Lower panel: Schematic positions of the centers of the Wannier functions in C and BN hexagons, and the projections of the *π* WF onto the nanotube axes. The positions of the centers of *σ* WF are indicated by circles, and those of *π* by squares. The direction of the shifts of *σ* and *π* WF in an adiabatic transformation from C to BN is indicated by arrows. The projections of shifts of the *σ* WF cancel, so that the *σ* WF do not contribute to polarization, (see text).

The σ-band WFs are centered in the middle of the C-C bonds in carbon nanotubes, while they are shifted towards the cations in BN nanotubes because of the different electronegativities of B and N atoms. Since these shifts have the same magnitude along each of the three bond directions, the vector sum of all shifts is zero, (see bottom panel of Figure 3), and the σ orbitals do not contribute to the total polarization of the system. The π-band WFs are centered on the cations in BNNTs, while in CNTs they have a peculiar V-shape, with centers somewhat outside of the C-C bond. The sum of the shifts of the π-band Wannier centers is non-zero only for the axial component, which means that the electronic polarization in BNNTs is purely axial.

The bottom panel of Figure 3 shows the projection of the π WF centers onto the axis of the tube. The projections of the centers have an effective periodicity of half of the axial lattice constant c, which leads to the indetermination of the electronic phase by multiples of π. Moreover, the WF description allows for an unambiguous unfolding of the electronic phase. In analogy to the ionic phase, we find that each individual hexagon carries a phase of $-\pi/3$, leading to a total electronic phase of $-n\pi/3$ for a, $(n, 0)$ nanotube. This result demonstrates that the

direction of the electronic polarization in a BNNT is specified by the orientation of the B-N bond and does not oscillate in direction with the nanotube diameter, contrary to the model Hamiltonian predictions.[7] We should point out that the Wannier function results are completely consistent with the Berry-phase calculations, since an electronic phase of $-n\pi/3$ for any n can be folded, modulo π, into the three families found previously.

When we combine the results for the ionic and electronic phases into a general formula for the phase of an arbitrary, (*n; m*) BNNT,

$$\Delta\Phi_z^{tot}(n,m) = \Delta\varphi_z^{ion}(n,m) + \Delta\varphi_z^{el}(n,m) = \frac{n-m}{3} - \frac{n-m}{3}, \quad (6)$$

we find that the two contributions cancel exactly and that the total spontaneous polarization in any BNNT is zero, i.e. the Wannier centers are arranged in such a way as to completely compensate the polarization due to ions. We have verified this result by two-point, (λ = 50 and 100%) calculations of the Berry phase difference for a number of chiral nanotubes, ((3,1),, (3,2),, (4,1),, (4,2),, (5,2), and, (8,2)) and found an exact cancellation in all BNNTs, except for those narrower than approximately 4 °A, where a residual polarization is present as an e®ect of the very high curvature. In such nanotubes Wannier centers cannot fully compensate the ionic polarization, due to the severe distortion of the atomic bonds, which makes these systems weakly pyroelectric. For example, P = 0.11 C/m^2 in, (3,0), 0.008 C/m^2 in, (7,0), and 0.002 C/m^2 in, (12,0) nanotubes.

Table 1. Piezoelectric properties of zigzag BNNT bundles.[38] The corresponding values for a few piezoelectric materials are listed for comparison.

(*n;m*)	diameter, (Å)	Z^*, (e)	$\|e_{33}\|$, (C/m^2)	Ref.
(5,0)	3.91	2.739	0.389	
(6,0)	4.69	2.696	0.332	
(7,0)	5.47	2.655	0.293	
(8,0)	6.24	2.639	0.263	
(9,0)	7.04	2.634	0.239	
(10,0)	7.83	2.626	0.224	
(11,0)	8.57	2.614	0.211	
(12,0)	9.38	2.609	0.198	
(13,0)	10.16	2.605	0.186	
w-AlN		2.653	1.50	[36]
w-ZnO		2.11	0.89	[35]
$PbTiO_3$			3.23	[2]
P(VDF/TrFE)			≈ 0.12	[3]

The exact cancellation is a result of the overall chiral symmetry of the nanotubes which, although not centrosymmetric, are intrinsically nonpolar. Nevertheless, cancellation of ionic and electronic polarizations is exact only in the limit of an isolated BNNT. The spontaneous polarization in a nanotube bundle, where the chiral symmetry is effectively broken, is different from zero. For example, in, (7,0) bundles at equilibrium distance of 3.2 Å $P \approx 0.01$ C/m^2. However, in this case it is hard to estimate the separate contributions to polarization due to bundling, extreme curvature and elastic deformation. Although smaller than in polymers or PZT, this polarization is comparable to some wurtzite pyroelectrics: *e.g.*, P = 0.06 C/m^2 in *w*-ZnO.[35]

We have also calculated the piezoelectric properties for various bundles comprised of zigzag BNNTs with individual diameters ranging from 3.9 to 10.2 Å. These results are summarized in Table 1 and compared to a few well-known piezo- and pyroelectric materials. While the piezoelectric constants of zigzag BNNTs are modest when compared with inorganic compounds, they are still substantially larger than those of commonly used polymers. Our current projects focus on evaluation and analysis of the factors responsible for pyro- and piezoelectric behavior of F- and Cl-based polymers, with the goal of identifying materials with much enhanced piezoelectric properties.

In summary, we have investigated the spontaneous polarization and piezoelectric properties of BN nanotubes using state-of-the-art *ab initio* methods. Our calculations demonstrate the complementary nature of Berry phase and Wannier function analysis, and show that a real-space description is necessary to unravel the Berry phases in complicated cases. The results suggest that BNNTs are excellent nonpolar piezoelectrics that exhibit substantially higher strain response than polar polymers. Moreover, we have shown that, contrary to the previous expectations, ideal non-interacting nanotubes are effectively nonpolar due to their intrinsic chiral symmetry, which leads to a total cancellation between the ionic and electronic polarizations. Breakage of this symmetry, as in the simple case of interacting nanotubes in a bundle, induces spontaneous polarization fields that are comparable to those of wurtzite semiconductors. Due to their piezo- and pyroelectric properties, BNNTs are excellent candidates for various nano-electro-mechanical applications.

4. Cyclopentene on Si(001)

Si(001) is known to undergo a dimer-row reconstruction. We first consider the adsorption of cyclopentene oriented parallel and perpendicular to the Si dimers. For acetylene on Si(001), these two adsorption geometries were found to be nearly degenerate energetically.[39] However, our results for the adsorption of cyclopentene show that the steric interactions between the larger C_5H_8 molecules strongly favor the parallel

configuration, at least for 1 ML coverage. The adsorption energy for the latter case is -0.5 eV per molecule, i.e., adsorption is not favorable. This agrees with the parallel orientation of the cyclopentene molecules observed by STM.[17]

For the parallel orientation of the molecule, we consider first the dimerized model. This configuration can be further classified according to the the positions of the hydrogen atoms in the immediate vicinity of the Si surface. In the 'trans-type' adsorption, the two H atoms are on alternating sides of the molecule, whereas both H atoms reside on the same side of the molecule in the 'cis-type' configuration. Apart from the positions of the downmost hydrogen atoms, the main structural difference between 'trans' and 'cis' configuration is in the orientation of the molecular C-C bonds near the interface. In the former case they are substantially twisted with respect to the Si dimer, as a consequence of the repulsive interactions between neighboring cyclopentene molecules. We calculate a rotation of 24° with respect to the direction of Si dimers. In addition, the Si dimers are slightly rotated with respect to the ideal direction. This is similar to the cases of C_2H_2 and C_2H_4 on the Si(001) surface,[40,41] in which the hydrogen atoms are twisted to reduce the repulsion between hydrogen charge clouds on neighboring molecules. In the present case, the twist is a consequence of repulsive interactions between the whole neighboring molecules. For the 'cis-type', there is no twist for the C-C bonds. In this case we calculate adsorption energies of 1.4 eV and 0.6 eV in LDA and GGA, respectively. Adsorption in 'trans-type' configuration leads to energy gains of 1.6 and 0.8 eV, calculated within LDA and GGA, respectively. Similarly, Akagi and Tsuneyuki[20] found for monolayer coverage the 'trans' configuration is favored over the 'cis-type' adsorption by 0.11 eV. In the following, we therefore focus on 'trans-type' adsorption. Its optimized structure is shown in Figure 4.

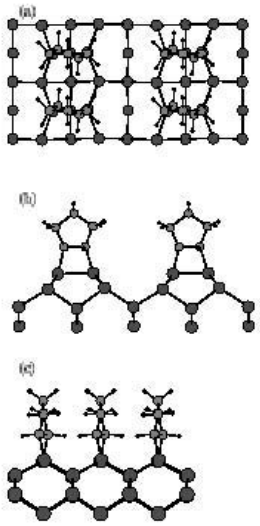

Figure 4. Optimized geometry for the 'trans-type' dimerized model of cyclopentene monolayer adsorption on Si(001):, (a) top view,, (b) and, (c) side views. Large, medium, and small circles represent silicon, carbon, and hydrogen atoms, respectively.

The cyclopentene molecules do not dissociate upon adsorption. However, the bond between the two carbon atoms attached to the surface is stretched. We calculate 1.38 and 1.51 Å for the gas-phase and the adsorbed molecules, respectively. The latter value is typical for single carbon bonds and indicates that the carbon atoms at the interface are sp^3 hybridized, rather than sp^2 as in the free molecule. The Si dimer length does not change significantly upon the adsorption of cyclopentene. The dimer buckling, however, is much reduced to only 1.3°. The Si-C bond length at the interface is 1.85 Å, similar to the bulk SiC bond length.

Even in the dimer-cleaved model, the cyclopentene molecules do not dissociate and the C-C bond near the interface is rotated by 24°. It is stretched to 1.56 Å and the originally dimerized Si atoms are now 4.3 Å apart. The Si-C bond length of 1.91 Å is slightly longer than the value of 1.85 Å in the dimerized model. The overall weaker interface bonding, together with the partially occupied Si dangling bonds, explain why the dimer-cleaved model is energetically less favored than the dimerized model, in spite of the lower interface strain. The calculated adsorption energies per molecule for the dimmer-cleaved model amount to 1.3 and 0.5 eV within LDA and GGA, respectively.

Compared to the adsorption of acetylene and ethylene, where the dimerized adsorption models are favored over the dimer-cleaved geometries by more than 1 eV,[42] the energy difference of 0.3 eV, (both in LDA and GGA) between the two adsorption geometries of

cyclopentene is relatively small. Both interface structures may thus occur at elevated temperatures. The most likely reaction pathway from the dimerized to the dimer-cleaved geometry is the breaking of the Si dimer. In Figure 5 we show the relative adsorption energy vs. the length of the Si dimer. In these calculations, we kept the coordinates of the Si surface atoms along the dimer direction fixed, while the remaining degrees of freedom and all the other atoms were allowed to relax. The energy barrier for the transition between the two structures is 0.85 eV in the LDA and 0.78 eV in the GGA. The two structures could thus co-exist at the interface, with the fraction of the dimerized model being much higher.

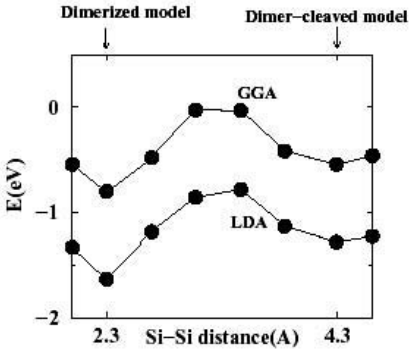

Figure 5.Adsorption energy vs. the Si-Si distance from LDA and GGA calculations. The circles represent the calculated energies and the solid lines are guides to the eye.

The interface geometry is very sensitive to the presence of hydrogen: if atomic hydrogen is added near the Si surface atoms, both the dimerized and the dimer-cleaved configurations relax towards the dimer-cleaved geometry with all dangling bonds saturated by H and a Si-Si distance of 3.8 Å. The hydrogen adsorption stabilizes the interface by releasing the large strain energy in the dimerized model or by saturating the dangling bonds in the dimer-cleaved model. The adsorption energy for the coadsorption system is defined by

$$\Delta E = -[E_{tot} - E(Si_{surf}) - E(C_5H_8) - E(H_2)]$$

where E_{tot} is the total energy of the total co-adsorbed system, $E(Si_{surf})$ is the energy of the clean Si surface, while $E(C_5H_8)$ and $E(H_2)$ are the energies of the respective gas-phase molecules. Neglecting temperature effects, our calculations for this system give adsorption energies of 2.8 eV within LDA and 2.7 eV within GGA. Due to the temperature and pressure dependence of the hydrogen chemical potential, (see, e.g., Ref. 43), the relative stability of the co-adsorbed system will strongly depend on the preparation conditions.

The saturation of the Si dangling bonds leads to an efficient electronic passivation: the interface electronic states are pushed out of the region of the Si bulk band gap. Some experimental evidence supporting the suggested co-adsorption of hydrogen – possibly released from fragmented molecules – is given by the observation of Si- H stretching vibrations in infrared spectroscopy.[9]

Turning to experimental verification of the predicted interface geometries by techniques like STM will be very difficult. However, one extremely structure-sensitive experimental technique, which is not restricted to ultrahigh vacuum conditions and can thus be used to monitor the interface formation *in situ*, is reflectance anisotropy spectroscopy (RAS), also termed reflectance difference spectroscopy (RDS).[44] Comparisons between the measured data and spectra computed for alternative structural models often allow for unambiguous determination of surface or interface geometries.[45,46]

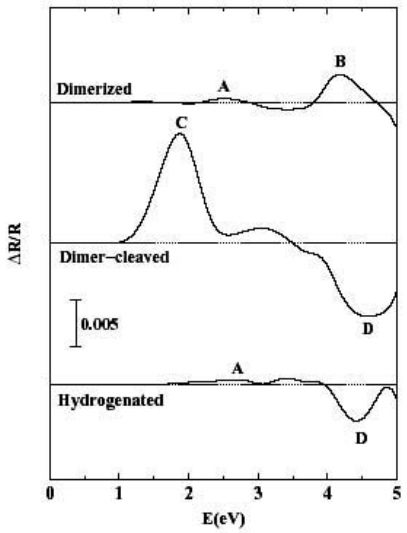

Figure 6. RAS spectra [($R_{[110]} - R_{[110]}$)/ = < *R* >] calculated for the dimerized model, the dimer-cleaved model, and the hydrogenated interface. Zero values are indicated by dashed lines.

Figure 6 shows RAS spectra calculated for the three 'trans-type' configurations studied here. In either case, the electronic transitions within the molecule do not contribute significantly to the interface optical properties in the energy range of up to 5 eV. This is expected, since each carbon atom in the cyclopentene molecule is sp^3-hybridized and chemically saturated. For the dimerized model, we only find a very weak shoulder A, which is due to optical anisotropies in the C_5H_8 overlayer. The peak B at the E_2 critical point energy of Si is related to electronic transitions between surface-modified bulk Si wave functions. This feature is typical for dimerized Si(001) surfaces.[47–49] The optical spectrum for the dimer-cleaved model is very different. Transitions involving the Si dangling bonds give rise to a strong anisotropy peak C at 2 eV, suppressing the weak signal from the C_5H_8

overlayer. For the hydrogenated interface, the weak signal from the C_5H_8 overlayer is again visible. For both the dimer-cleaved and the hydrogenated interface models a negative anisotropy D is observed at the E_2 critical point energy of Si. The change from positive to negative optical anisotropies upon dimmer-cleavage at the E_2 energy calculated here, (features B and D) has been previously observed in experiments for hydrogenated Si surfaces.[50]

In summary, we investigated the atomic structure and surface optical properties of the Si(001):C_5H_8 interface, using the real-space multigrid DFT method within both the local density and the generalized gradient approximations. While the adsorption energy depends on the choice of the exchange-correlation approximation, the relative stabilities of the different models have the same trends in both LDA and GGA calculations. The formation of a dimerized structure via the [2+2] cycloaddition reaction is favored over the breaking of the surface Si dimer. The adsorption of additional hydrogen atoms increases the stability of the interface by releasing the strain energy and saturating the dangling bonds. The resulting surface is electronically well passivated. We found strong and structure-dependent surface optical anisotropies, which mainly arise from electronic transitions within the substrate and between the substrate and the overlayer. Even a discrimination between 'cis' and 'trans'-type adsorption configurations is possible, based on measurements of the reflectance anisotropy. Surface optical spectroscopies are therefore well suited for monitoring the formation of interfaces between Si surfaces and hydrocarbon overlayers, as well as for determining the structure of the overlayer.

5. Significance to DoD

Our research investigates advanced materials and processes that will in due course lead to new military applications and potentially even paradigm shifts. In the area of nanotubes, we have shown that BN nanotubes are excellent candidates for piezoelectric sensors and actuators. They are already known to be extraordinarily strong and inert, and they could find widespread use in nano-electromechanical switches and sensors. Another important potential application is in sonar equipment, which currently utilizes polar polymers. The mechanical properties of polymer mixtures could be substantially strengthened by the addition of crosslinked nanotubes, and BN nanotubes would also increase the piezoelectric response. Our current work addresses the pyro- and piezoelectric response of polymers, in an effort to arrive at a comprehensive understanding of lightweight piezoelectric materials. Other potential applications of BN/C nanotubes include high efficiency electron emitters for microwave amplifiers and high-resolution flat panel displays.

The second part of our work deals with advanced processing and development of semiconductor materials. Optical monitoring of surface structures enable *in situ* observation and real-time feedback control of the growth of device structures with nearly monolayer resolution. However, the optical "fingerprints" corresponding to different surface structures must first be computed and understood. We have developed a unique method for accurate computations of surface optical spectra and are applying it to important benchmark systems. The adsorption of cyclopentene on Si(001), which is the standard growth face of Si, enables for controlled further attachment of organic ligands, including DNA. Potential applications include the integration of Si electronics with organic sensor structures, able to detect minute amounts of specific compounds or microorganisms. However, in order to engineer appropriate, electrically active molecular 'connectors' between the organic and Si parts of the device, the interface structure must be thoroughly understood. Our current work examined various alternative structures, identified the lowest energy structures for both pristine and hydrogenated interfaces, and computed their optical signatures for experimental verification.

6. Systems Used

NAVO SP3; ERDC T3E

7. CTA

CEN 60%; CCM 40%

References

[1] T. Kumazawa *et al.*, *Appl. Phys. Lett.*, 72, 1998, p. 608; T. Yamamoto, *Jpn. J. Appl. Phys.*, 37, 1998, p. 6041.

[2] G. Sághi-Szabó, R.E. Cohen. and H. Krakauer, *Phys. Rev. Lett.*, 80, 1998, p. 4321 , *Phys. Rev. B*, 59, 1999, p. 12771.

[3] T. Furukawa, *IEEE Trans. Electr. Insul.,* 24, 1989, p. 375; G. Eberle, H. Schmidt, and W. Eisenmenger, *IEEE Trans. Diel. Electr. Insul.*, 3, 1996, p. 624.

[4] A. Rubio, J.L. Corkill, and M.L. Cohen, *Phys. Rev. B*, 8 49, 1994, p. 5081; X. Blase *et al.*, *Europhys. Lett.*, 28, 1994, p. 335.

[5] N.G. Chopra *et al.*, *Science*, 266, 966, 1995, p. ; A. Loiseau *et al., Phys. Rev. Lett.*, 76, 1996, p. 4737.

[6] P. Zhang and V.H. Crespi, *Phys. Rev. B*, 62, 2000, p. 11050; H.F. Bettinger *et al. ibid.* 65, 2002, p. 041406.

[7] E.J. Mele and P. Král, *Phys. Rev. Lett.*, 88, 2002, p. 056803.

[8] J. Dabrowski and H.-J. M¨ussig, *Silicon Surfaces and Formation of Interfaces,* World Scientific, Singapore, 2000, and references therein.

[9] R.J. Hamers, J.S. Hovis, S. Lee, H. Liu, and J. Shan, *J. Phys. Chem. B*, 101, 1997, p. 1489.

[10] J.T. Yates Jr., *Science*, 279, 1998, p. 335.

[11] J.S. Hovis, S. Lee, H. B. Liu, and R. J. Hamers, *J. Vac. Sci. Technol.*, B 15, 1997, p. 1153.

[12] J.S. Hovis and R.J. Hamers, *J. Phys. Chem. B*, 102, 1998, p. 687.

[13] J.S. Hovis, H. Liu, and R.J. Hamers, *J. Phys. Chem. B*, 102, 1998, p. 6873.

[14] R. Akiyama, T. Matsumoto, and T. Kawai, *Phys. Rev. B*, 62, 2000, p. 2034.

[15] R.J. Hamers, J.S. Hovis, C.M. Greenlief, and D.F. Padowitz, *Jpn. J. Appl. Phys.*, 38, 1999, p. 3879.

[16] J.S. Hovis, H. Liu, and R.J. Hamers, *Surf. Sci.*, 1, 1998, pp. 402–404.

[17] J.S. Hovis, H. Liu, and R.J. Hamers, *Appl. Phys. A: Mat. Sci. Proc.*, 66, 1998, p. S553.

[18] S.W. Lee, J.S. Hovis, S.K. Coulter, R.J. Hamers, and C.M. Greenlief, *Surf. Sci.*, 462, 2000, p. 6.

[19] H. B. Liu and R. J. Hamers, *Surf. Sci*,. 416, 1998, p. 354.

[20] K. Akagi and S. Tsuneyuki, *Surf. Sci.*, 493, 2001, p. 131.

[21] J. Cho and L. Kleinman, *Phys. Rev. B*, 64, 2001, p. 235420.

[22] N. Pernodet, V. Samuilov, K. Shin, J. Sokolov, M.H. Rafailovich, D. Gersappe, and B. Chu, *Phys. Rev. Lett.*, 85, 2000, p. 5651.

[23] T. Strother, R.J. Hamers, and L.M. Smith, *Nucleic Acids Research*, 28, 2000, p. 3535.

[24] R. Koneeny and D. J. Doren, *J. Am. Chem. Soc*., 119, 1997, p. 11098.

[25] E.L. Briggs, D.J. Sullivan, and J. Bernholc, *Phys. Rev. B*, 54, 1996, p. 14362.

[26] J.P. Perdew and A. Zunger, *Phys. Rev. B*, 23, 1981, p. 5048.

[27] J.P. Perdew, K. Burke, and M. Ernzerhof, *Phys. Rev. Lett.*, 77, 1996, p. 3865.

[28] D.R. Hamann, *Phys. Rev. B*, 40, 1989, p. 2980; L. Kleinman and D.M. Bylander, *Phys. Rev. Lett.*, 48, 1982, p. 1425.

[29] R.D. King-Smith and D. Vanderbilt, *Phys. Rev. B*, 47, 1993, p. 1651; D. Vanderbilt and R.D. King-Smith *ibid.* 48, 1993, p. 4442.

[30] R. Resta, *Rev. Mod. Phys.*, 66, 1994, p. 899.

[31] D. Vanderbilt, *J. Phys. Chem. Solids*, 61, 2000, p. 147.

[32] R. Del Sole, *Solid State Commun.*, 37, 1981, p. 537.

[33] F. Manghi, R. Del Sole, A. Selloni, and E. Molinari, *Phys. Rev. B*, 41, 1990, p. 9935.

[34] A.I. Shkrebtii, N. Esser, W. Richter, W.G. Schmidt, F. Bechstedt, B.O. Fimland, A. Kley, and R. Del Sole, *Phys. Rev. Lett.*, 81, 1998, p. 721.

[35] F. Bernardini, V. Fiorentini, and D. Vanderbilt, *Phys. Rev. B*, 56, 1997, p. R10024; *ibid.* 63, , 2001, p. 193201.

[36] A. Zoroddu *et al.*, *Phys. Rev. B*, 64, 2001, p. 045208.

[37] In the limiting case of flat C or BN sheets, the electronic polarization is zero for any value of λ, due to the existence of a threefold symmetry axis perpendicular to the surface of the sheet.

[38] The data reported in Table 1 for nanotube bundles assume a close-packed geometry with intertube equilibrium distance of 3.2 Å.

[39] W.A. Hofer, A.J. Fisher, and R.A.Wolkow, *Surf. Sci.*, 475, 2001, p. 83.

[40] W. Widdra, A. Fink, S. Gokhale, P. Trischberger, D. Menzel, U. Birkenheuer, U. Gutdeutsch, and N. Rosch, Phys. Rev. Lett. 80, 1998, p. 4269.

[41] U. Birkenheuer, U. Gutdeutsch, N. Rösch, A. Fink, S. Gokhale, D. Menzel, P. Trischberger, and W. Widdra, *J. Chem. Phys.*, 108, 1998, p. 9868.

[42] J.H. Cho, L. Kleinman, C. T. Chan, and K. S. Kim, Phys. Rev. B 63, 073306, 2001, p. 073306; and references therein.

[43] C.G. Van de Walle and J. Neugebauer, *Phys. Rev. Lett.*, 88, 2002, p. 066103.

[44] D.E. Aspnes and A.A. Studna, *Phys. Rev. Lett.*, 54, 1985, p. 1956.

[45] W. Lu, W.G. Schmidt, E.L. Briggs, and J. Bernholc, *Phys. Rev. Lett.*, 85, 2000, p. 4381.

[46] J R. Power, P. Weightman, S. Bose, A.I. Shkrebtii, and R. Del Sole, *Phys. Rev. Lett.*, 80, 1998, p. 3133.

[47] L. Kipp, D.K. Biegelsen, J.E. Northrup, L.-E. Swartz, and R.D. Bringans, *Phys. Rev. Lett.*, 76, 1996, 2810p. .

[48] M. Palummo, G. Onida, R. Del Sole, and B. S. Mendoza, *Phys. Rev. B*, 60, 1999, p. 2522.

[49] W.G. Schmidt, F. Bechstedt, and J. Bernholc, *Phys. Rev. B*, 63, 2001, p. 045322.

[50] R. Shioda and J. van der Weide, *Appl. Surf. Sci.*, 266, 1998, pp. 130–132.